NUCLEAR INSTRUMENTS AND METHODS 162 (1979) 161-180 ; © NORTH-HOLLAND PUBLISHING CO.

IV. Magnetic detectors: Heavy charged particles

MAGNETIC SPECTROGRAPHS FOR NUCLEAR REACTION STUDIES

HARALD A. ENGE

Laboratory for Nuclear Science, Massachusetts Institute of Technology, Cambridge, MA 02139, U.S.A.

A brief introduction is given to the terminology of ion optics as applied to magnetic spectrographs. First-order resolving power and aberration-limited resolving power are defined. Several examples of magnetic spectrographs are described and the main characteristics tabulated. Kinematic broadening and means of correcting it are discussed. Limitations to the final resolution imposed by target rather than spectrograph effects are treated next with special emphasis on heavy-ion reactions. Finally, one example of a multigap spectrograph is described.

1. Introduction

Magnetic spectroscopy of nuclear particles is as old as nuclear physics itself. In 1899 Becquerel used what we would call a 180° single-focusing magnetic spectrograph to show that beta radiation is "soft". In the Rutherford era several magnetic spectrographs were employed in the study of natural alpha decay. One of these instruments was a single-focusing 180° spectrograph with high resolution and accuracy[1]).

In the early forties R. J. Van de Graaff and W. W. Buechner, at MIT, saw the need for high resolution spectroscopy of particles emitted in nuclear reactions and initiated the design of an instrument which was basically a copy of Rutherford's alpha-particle spectrograph. Because of the war, the project was put aside and the instrument was not finished before 1948. At about the same time, a different type of spectrograph was built by C. C. Lauritsen's group at the California Institute of Technology. Both the MIT magnet and the Cal Tech magnet were mounted in the target rooms of Van de Graaff accelerators and used for determining energies of charged particles emitted in nuclear reactions. Both instruments are described briefly in a later section of this paper.

2. Charged-particle dynamics

The force on a particle of charge Q and velocity v moving through a magnetic field B is given by:

$$F = Qv \times B. \tag{1}$$

Since the magnetic force is always perpendicular to the direction of motion of the particle, it does not change its kinetic energy. Therefore, the mass of the particle does not change either, during the motion through a magnetic field. The magnetic force produces a centripetal acceleration, and assuming for simplicity that the velocity is perpendicular to the magnetic field, we get

$$mv^2/\rho = QvB, \tag{2}$$

where ρ is the orbit radius. Eq. (2) reduces to

$$B\rho = mv/Q. \tag{3}$$

This equation is relativistically correct with m being the relativistic mass. The product $B\rho$ is called the *magnetic rigidity* of the particle. The relationship between the momentum $p = mv$ and the magnetic rigidity is, of course, the basis for magnetic spectroscopy.

Some convenient formulas for the magnetic rigidity (measured in kG·cm) are given below. First:

$$B\rho = \frac{3.3356}{q}(pc)\ \text{kG}\cdot\text{cm}, \tag{4}$$

where (pc) measured in MeV is the momentum times the velocity of light and q is the charge *state* $q = Q/e$, i.e., the number of elementary charges e carried by the particle. The product (pc) is sometimes called the momentum in MeV/c. By introducing the relativistic relationship between the kinetic energy E_K (MeV) and the momentum, we obtain

$$B\rho = \frac{3.3356}{q}\sqrt{(2m_0c^2E_K + E_K^2)}\ \text{kG}\cdot\text{cm}. \tag{4a}$$

For non-relativistic particles, this can be reduced to

$$B\rho = \frac{143.97}{q}\sqrt{(ME_K)}\ \text{kG}\cdot\text{cm}, \tag{4b}$$

where M is the mass of the particle in atomic mass units. ME_K/q^2 is called the *mass-energy product.*

3. General spectrograph requirements

The main task for the spectrograph designer is clearly to produce an instrument in which particles of different momenta (magnetic rigidities) are spatially separated on a position-sensitive detector after passing through the magnetic field region or regions. Coupled with this is the requirement that particles emitted into as large a solid angle as possible must be accepted from the source (target) in order to avoid excessive exposure times. What is required is some precision ion optical focusing such that particles emitted into a given solid angle and having the same momentum are focused to a small spot or line on the detector. The most difficult problem, then, turns out to be to minimize aberrations in this imaging process such that the largest possible solid angle can be utilized. At the same time the range of momenta covered by the spectrograph should be sufficiently large to avoid the necessity of multiple exposures with different settings of the magnetic field in order to cover the total energy range desired. Finally the ability of the instrument to resolve groups of particles with small momentum differences depends upon the instrument's ion-optical magnification and momentum dispersion. This is discussed in more detail below.

4. Ion optics of spectrographs

In discussing ion optical devices, we borrow the terminology from light optics. Words such as focusing, dispersion, focal lengths, principal planes, resolution, etc. have all the same meaning in ion optics as in light optics. A convex glass lens has the property that light rays passing through it are deflected towards the axis by an angle that to first order is proportional to the distance from the center of the lens. As a result, a bundle of parallel rays converges towards a point after passing the lens. Ion optical lenses, i.e. solenoids, quadrupole lenses and deflecting magnets, focus bundles of ions in much the same way, but with some complications. A solenoid twists the beam as it focuses, and a quadrupole or the fringing fields of a deflecting magnet act as a converging lens in one plane and a diverging lens in a plane perpendicular thereto.

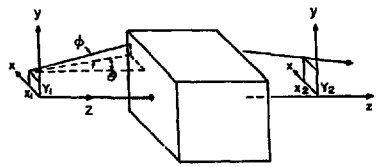

Fig. 1. Coordinate systems used in calculations of ion-beam transfers.

In order to describe what happens to a bundle of ion rays passing through one or more ion-optical devices, we introduce the concept of *transfer coefficients*. The box in fig. 1 represents any ion-optical transfer system consisting of dipoles, quadrupoles, solenoids, and higher order multipoles. Electrostatic devices may also in principle be included, but we will here assume that no net gain in momentum results. A particle is assumed to be emitted from (or passing through) point x_1, y_1 in the plane $z_1 = 0$. After having traversed the system, it will be detected at position x_2, y_2 in the plane $z_2 = 0$. The direction of the particle before entering the system is specified by the angles θ and ϕ defined in the figure. A reference momentum p_0 is assumed and the deviation from this momentum is given as $\delta = \Delta p/p_0$. For simplicity, we shall in the following discussion assume that the system is mechanically symmetric about a plane assumed to be the xz plane and that the magnetic field is everywhere perpendicular to the symmetry plane. This then will have to be the median plane of any dipole magnet (deflecting magnet) and a symmetry plane between poles of any quadrupole or higher order multipole magnet. Solenoids violate the condition but can under certain circumstances be included if the appropriate rotation of the coordinate system is performed.

The position at the exit is clearly a function of the position and direction at the entrance and of the momentum. Thus,

$$x_2 = f(x_1, \theta_1, y_1, \phi_1, \delta) \tag{5}$$

with similar expressions for y_2, θ_2, and ϕ_2. We now assume that the exit coordinate system has been placed such that a particle with momentum p_0 emitted along the z_1 axis exits along the z_2 axis. We can then express eq. (5) as a Taylor expansion in x_1, θ_1, y_1, ϕ_1, and δ. The quantities x_1 and y_1 are presumably small (relative to, for instance, the orbit radius in a dipole) because they represent target spot size. The angles θ_1 and ϕ_1 are generally less than 0.1 rad. For a broad-range spectrograph, δ is not necessarily small; however, we will assume that we expand only for a small range about the reference momentum p_0 and then repeat the

calculations for different values of the reference momentum. This means moving the exit coordinate system to new positions, presumably along a focal plane or focal surface. The Taylor expansion of eq. (5) can be written as

$$\frac{x_2}{\rho} = (x/x)\frac{x_1}{\rho} + (x/\theta)\,\theta_1 + (x/\delta)\,\delta + \\ + (x/x^2)\frac{x_1^2}{\rho^2} + (x/x\theta)\frac{x_1}{\rho}\theta_1 + (x/\theta^2)\,\theta_1^2 + \\ + (x/x\delta)\frac{x_1}{\rho}\delta + (x/\theta\delta)\,\theta_1\delta + (x/\delta^2)\,\delta^2 + \\ + (x/y^2)\frac{y_1^2}{\rho^2} + (x/y\phi)\frac{y_1}{\rho}\phi_1 + (x/\phi^2)\,\phi_1^2 + \\ + \text{higher order terms}. \qquad (6)$$

Eq. (6) has been written in a non-dimensional form in that x and y have been divided by the orbit radius ρ of the ray with momentum p_0 in a representative dipole. The factor (x/x) is called a transfer coefficient and is actually the first-order derivative $\partial x_2/\partial x_1$. Similarly, the term (x/θ) is equal to $\partial x_2/\partial\theta_1$, etc. The term (x/x) is the magnification of the system in the x direction and (x/δ) is the dispersion; it measures the displacement in the x direction at the exit per unit change in δ. Because of the assumed symmetry about the median plane, terms of the form $(x/y^n\phi^m)$ are zero unless the sum $n+m$ is even. Therefore, there is no such term as (x/ϕ) in eq. (6).

The function [eq. (5)] is not normally a determinable analytic function. The Taylor expansion is therefore not performed in the conventional way by taking analytic derivatives. Rather, it is done by numerical techniques. The first and second order coefficients can be determined for a system consisting of an arbitrary number of elements by a matrix multiplication computer program TRANSPORT[2]) developed by K. L. Brown and coworkers. Coefficients up to fifth order can be determined by use of the program RAYTRACE[3]) in which a number of trajectories through the system are determined by integration of the equations of motion.

We will now assume that the exit coordinate system is placed at the position where $(x/\theta)=0$. This, by definition, is the position of first-order focus. We will further assume that the target spot size is small enough so that we can neglect any term in x_1 except the first-order term (the magnification). We can then rewrite eq. (6) in the following form:

$$\frac{x_2}{\rho} = (x/x)\frac{x_1}{\rho} + (x/\delta)\,\delta + \\ + (x/\theta^2)\,\theta^2 + (x/\theta\delta)\,\theta\delta + (x/\phi^2)\,\phi^2 + (x/\delta^2)\,\delta^2 + \\ + \text{higher order terms}. \qquad (7)$$

We now define the first-order resolving power of the system as the inverse of the fractional change in momentum needed to displace the first-order image a distance equal to its width. The first order image width is $\Delta x_2 = M_x \Delta x_1$ where the magnification is $M_x \equiv |(x/x)|$. A momentum change $\delta = \Delta p/p_0$ displaces the image by $\Delta x_2 = \rho D\delta$ where the dispersion is $D \equiv |(x/\delta)|$. Hence,

$$\mathscr{R}_1 = \frac{p}{\Delta p} = \delta^{-1} = \frac{D\rho}{M_x \Delta x_1}. \qquad (8)$$

For a broad-range spectrograph D/M_x should be treated as a function of ρ, often increasing with ρ. The best first-order resolving power is then clearly obtained at the upper end of the range.

Proceeding now to the higher-order terms in eq. (7), we note first that the term (x/θ^2) and others of the form (x/δ^n) produce a non-linearity in the dispersion. This may or may not be desirable. For this discussion, however, it is important to notice that these terms do not produce aberrations of the image in the same way, as for instance (x/θ^2).

The term $(x/\theta\delta)$ can be shown to be related to the focal plane angle, i.e. the angle ψ between the z_2-axis and the normal to the focal surface. The relationship is

$$\tan\psi = -\frac{(x/\delta)}{(\theta/\theta)\,(x/\delta)}. \qquad (9)$$

Higher order terms of the form $(x/\theta\delta^n)$ produce curvatures of the focal surface and again this may or may not be desirable.

The most important higher order terms are the aberration terms (x/θ^2), (x/ϕ^2), (x/θ^3), (x/ϕ^2), etc., because they blur the image formed of the object (target spot) by particles of identical momenta. If Δx_{ab} represents an appropriate measure of the blurring of the image by these aberration terms, the obtainable resolving power (assuming a point object) is

$$\mathscr{R}_{ab} = \frac{D\rho}{\Delta x_{ab}}. \qquad (10)$$

The full width at half maximum (fwhm) of a peak representing the intensity distribution on the detector is normally used to define resolving power. However, the fwhm is a meaningless measure for the aberration contribution alone (it is zero because the peak height is infinite). Folded with other contributions, such as first-order image width, target thickness effect, energy fluctuation of the primary beam, etc., the aberrations, of course, do contribute to the fwhm. The quantity that is easiest to calculate for the aberration term is the full width at the *base* of a peak, Δx_{base}. For simplicity we propose to use $\Delta x_{\text{ab}} = \frac{1}{2}\Delta x_{\text{base}}$.

The properties of the spectrograph in the dispersive x-direction are, of course, most important because they determine the resolving power. The aberrations in the y-direction have to be watched too, however, for a double-focusing instrument. Generally, the requirement is that all particles accepted by the entrance solid angle of the spectrograph must fall within a detector window of reasonable width (typically a few centimeters). Clearly, the double-focusing (stigmatic) condition $(x/\theta) = 0$ and $(y/\phi) = 0$ has to be met for some intermediate momentum. For a broad-range instrument it is next important that $(y/\phi\delta) = 0$ or small as determined along the x focal surface (rather than in a fixed plane $z_2 = 0$). This was one of the major design factors for the split-pole spectrograph discussed below. The only other important second-order term affecting y-focusing is $(y/\theta\phi)$. Fortunately, this term is coupled to (x/ϕ^2) and is always small for a double-focusing instrument if (x/ϕ^2) is small.

5. Examples of single gap spectrographs

The basic layout of the MIT spectrograph[4]) mentioned in the introduction is shown in fig. 2. The instrument was called the annular magnet because an annular airgap region (or half of it) was used. The return yoke is in the center of the device. The beam struk the target perpendicular to the median plane of the spectrograph and the reaction products were therefore only detected at an angle of 90° from the beam. Detectors were nuclear track plates which subsequently were developed and analyzed under a microscope. The momentum range of the instrument was $p_{\max}/p_{\min} = 1.04$ and the solid angle was approximately 0.5 msr (millisteradian). A momentum resolving power of $\mathscr{R} \approx 1600$ was achieved[5]). A 180° instrument has the great advantage that the diameter of the particle orbit can be measured more or less directly so that with an absolute measurement of the magnetic field no auxilliary means are necessary for calibrating the instrument. However, the spectrograph described was launched before the advent of the NMR fluxmeter. Polonium alpha particles were therefore used as a calibration source.

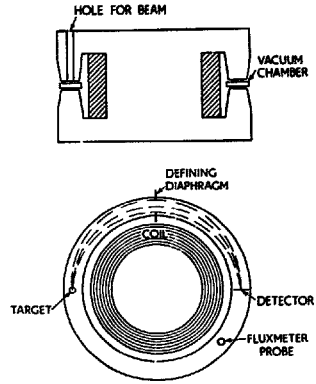

Fig. 2. The annular magnet used in conjunction with the MIT 2 MeV (open air) Van de Graaff accelerator. Restricted to reaction angle $\theta_R = 90°$.

The most important features of the annular magnet and other spectrographs mentioned in this section are listed in table 1. The airgap d and the "layout" radius R (usually $R = \rho_{\text{mean}}$) are given for the original instrument in each case. All of the spectrographs can, of course, be scaled up or down; for the more sophisticated types, however, only by maintaining a constant d/R ratio. The aberration-limited resolving powers $\mathscr{R}_{\text{ab}}$ listed are approximate values as determined at the nominal solid angle Ω, which is not necessarily the maximum solid angle in each case.

The final entry in table 1 is a number Q which roughly expresses the data-taking power of the spectrograph. It is defined as $Q \equiv \Omega/n$ where Ω is the acceptance solid angle in msr and n is the number of exposures needed to cover a momentum range of a factor two, i.e.,

$$Q = \frac{\Omega \ln(p_{\max}/p_{\min})}{\ln 2} \qquad (11)$$

TABLE 1
Single gap spectrographs.

Spectrograph	Mean radius R (cm)	Airgap d (cm)	Range p_{max}/p_{min}	Solid angle Ω (msr)	Dispersion $D = \Delta x/\Delta p$	Magnif. M_x	M_y	D/M_x	Res. pow.[a] (approx.) $\mathcal{R}_{ab}$	Focal ψ (degrees)	Surface shape	Kinemtaic correction	Q (msr)
Annular magnet[4])	35	1.3	1.04	0.5	2.0	1.0	–	2.0	2000	0	Straight	None	0.03
Michigan $n=\frac{1}{2}$[7])	133		1.06	0.4	4.0	1.0	1.0	4.0	8000	55	Straight	Det. displ.	0.03
Browne–Buechner[8])	51	1.3	1.5	0.4	2.0	1.0	–	2.0	3000	63.5	Curved	None	0.23
Elbek[11])	62	2.8	2.1	1.0	2.4	0.8	–	3.0	4500	45.2	Curved	Det. displ.	1.1
Split-pole[12])	60	3.8	2.8	2.0	1.9	0.3	4.0	5.7	4500	41.5	Curved	Det. displ.	3.0
Berkeley[14])	178	10.0	1.15	1.0	2.1	0.4	5.0	5.3	5000	0	Curved	Det. displ.	0.20
Q3D[16])	100	8.0	1.10	14.7	14.0	1.5	4.0	9.5	10 000	43.0	Curved	Multipole	2.0
Q3D II[18])	90	7.2	1.22	14.7	10.2	1.1	3.0	9.0	10 000	43.0	Curved	Multipole	4.2
QWTH[19])	90	7.2	1.28	10.0	7.8	1.1	4.3	7.3	10 000	45.0	Straight	Multipole	3.6
QMG[20])	120	9.6	1.10	10.0	6.7	0.9	5.8	7.1	10 000	45.0	Straight	Multipole	1.4
Indiana QDQ[22])	135	8.0	1.03	3.2	7.7	1.0	1.0	7.7	6000	46.0	Curved	Multipole	0.14
Osaka QDDQ[23])	150	8.0	1.06	13	11.1	1.1	4.0	10.0	10 000	52	Curved	Multipole	1.1
GSI QQDQ[24])	200	10.8	1.08–1.29	3.0	2.6–0.7	1.8–0.26	2–7	2.9–5.5	370	Variable	–	Quadrupole	.3–1.1
Jülich QQDQ[25])	172	6.0	1.10	10.0	9.8	0.9	7.2	11.5	?	0	Curved	Multipole	0.7
QSP design[26])	100	8.0	1.86	8.8	2.1	0.3	3.3	7.1	2500	38.3	Straight	Det displ.	7.9
Tokyo QDD[27])	140	10.0	1.15	6.4	2.8	0.38	4.4	7.4	?	55.0	Curved	Det. displ.	1.3
IKO QDQ[28])	180	14.4	1.10	17.2	4.6	1.2	2.5	3.9	4000	38.7	Straight	Computer	2.4
Indiana QQSP[29])	38	5.8	1.63	<35.0	2.3	0.3	3.3	7.4	1000[b]	40.5	Straight	Computer	20.0
Bates QQSP[30])	50	5.0	1.22	35.0	2.5	0.4	4.2	6.5	2000	46.1	Curved	Computer	10.0
Rochester QD[31])	75	35	1.5	<400	–	–	–	–	3000	–	–	Computer	<200

[a] An approximate measure of the theoretical aberration-limited resolving power at the solid-angle listed.
[b] With data corrected for (x/θ^3).

Almost simultaneously with the publication of the first description of the MIT instrument, a report was given on a double-focusing spectrometer designed by C. C. Lauritsen's group[6]) at the Kellogg Laboratory of California Institute of Technology. The instrument featured an inhomogeneous magnetic field that provides stigmatic (double) focusing $(x/\theta = 0$ and $y/\phi \approx 0)$ as in a betatron. However, the target and detector were outside the magnetic field in the Kellogg instrument and approximate stigmatic focusing was accomplished at 180° deflection by appropriate selection of the distance from the target to the spectrograph and the distance from the spectrograph to the detector. A more modern version of this type of instrument was in use until recently at the University of Michigan[7]).

A large stepup in data-taking power was achieved by the introduction of the MIT broad-range spectrograph[8]) (the Browne–Buechner spectrograph) shown in fig. 3. The instrument is basically a 90° sector magnet familiar from several mass spectrographs. However, it has circular pole boundaries and this offers two advantages for this type of instrument. First, the aberration term (x/θ^2) is zero for the particles that are deflected by 90° and tolerably small for other momenta. Secondly, but less important, the circular geometry

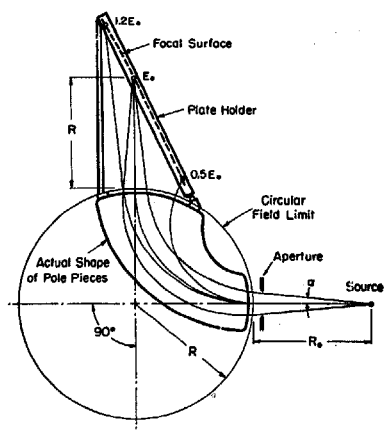

Fig. 3. The first broad-range spectrograph, the Browne–Buechner spectrograph.

causes the central ray to enter and exit the magnetic field perpendicular to the boundary for all momenta. This means that all momenta experience the same amount of transverse focusing – namely, none (or, strictly speaking, a small amount of defocusing). The momentum range of the instrument is approximately $p_{max}/p_{min} = 1.5$.

The Browne–Buechner spectrograph has been copied in many laboratories throughout the world and has been one of the important workhorses in nuclear reaction studies. A modification of it was designed for Chalk River Laboratories in Canada[9]). A quadrupole placed between the target and the dipole increased the solid angle to about 8 msr. The original MIT spectrograph was eventually also outfitted with a quadrupole mounted

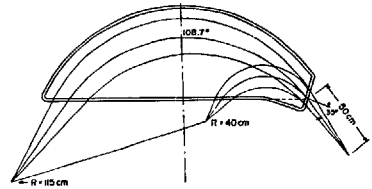

Fig. 4. A broad-range spectrograph devised by B. Elbek (Oak Ridge version). It has very good correction for (x/θ^2) over the whole range. It is not stigmatically focusing.

such that it could be twisted about its axis for kinematic correction[10]) (cf. section 6.)

An improved broad-range spectrograph was de-

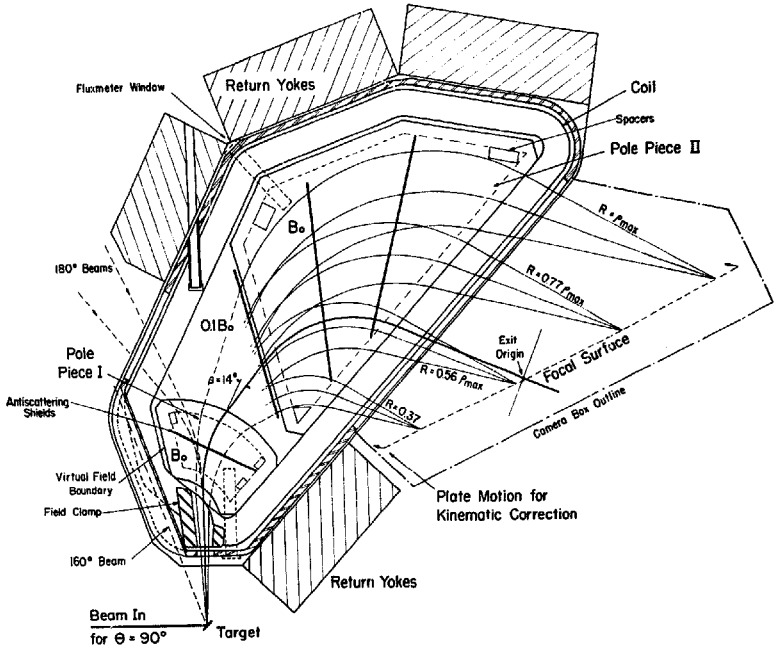

Fig. 5. The split-pole spectrograph. It has two sets of pole pieces magnetized by the same set of coils. It has good second-order correction and is stigmatically focusing over the whole range.

signed by Elbek[11]) and coworkers (fig. 4.) The entrance angle of 35° provides some transverse focusing, not enough to make the instrument stigmatic, but the transverse focusing increases the solid angle accepted by the instrument by about a factor 1.5. The most important feature of the Elbek spectrograph is that it has good second-order correction ($x/\theta^2 \approx 0$) over the entire range. The focal surface is slightly curved, as it is on most broad-range instruments, but no more than can be tolerated by the nuclear track plate detectors.

The basic ideas of focusing utilized in the Elbek instrument were modified and carried a bit further in the split-pole[12]) spectrograph (fig. 5). This instrument has two sets of pole pieces and the two boundaries facing each other in the "split" are shaped such that approximate transverse focusing is accomplished over the full range at the same time as second-order correction is maintained ($x/\theta^2 \approx 0$ and $x/\phi^2 \approx 0$). The transverse focusing is good enough such that particles that more or less fill a 3.8 cm gap fall well within a 1 cm wide strip on the detector. The split-pole is designed to accept particles within a solid angle of 8–12 msr, depending upon momentum. However, the resolution deteriorates rapidly above 2 msr because of the magnitude of the (x/θ^3) aberration term. DeVries and coworkers[13]) have demonstrated that by measuring the angle θ_2 with the aid of a second detector plane, and correcting the data obtained for (x/θ^3), good resolution can be obtained at full solid angle.

An instrument that was especially designed for heavy-ion work was built at Berkeley by Hendrie and co-workers[14]) (fig. 6). The focal surface is approximately normal to the central ray of the instrument such that heavy ions going through the detector window lose a minimum amount of energy and are less subject to scattering. To accomplish this, it has been necessary to make the exit boundary of the magnet concave as shown in the figure. This has the effect of driving the aberration coefficient (x/θ^2) strongly negative. To remedy this a sextupole element is inserted between the quadrupole and the dipole.

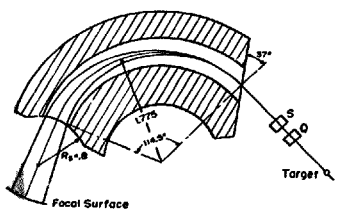

Fig. 6. The Berkeley heavy-ion spectrograph. Q=quadrupole, S=sextupole.

With the development of multiwire proportional counters of various kinds, it became important to produce magnetic spectrographs to match the position resolution of these devices. At the suggestion of the Tandem Group at the Max Planck Institut für Kernphysik, the present author started some calculations which eventually resulted in a series of instruments called the Q3D's. A basic difference between the Q3D's and all instruments described above is that a transverse (y-direction) image is formed in the middle of the spectrograph ($y/\phi = 0$), and this is again reimaged at the detector. The effect of this is that it is considerably easier to correct for aberrations, both of second and higher order. Although the actual situation is a bit more complex than this, one can say that basically the aberration coefficients caused by off-median plane motion (such as x/ϕ^2) are corrected where the amplitudes in the y-direction are large. The median plane aberration coefficients, such as (x/θ^2) through (x/θ^5), are corrected close to the middle of the instrument where the x amplitude is large and the y amplitude is small. The result is that it is possible to obtain a resolving power $\mathcal{R}_{ab} > 10^4$ for solid angles of 10–15 msr.

Fig. 7 shows the layout of Q3DI[15,16]) (Heidelberg, München, Princeton). The element between D1 and D2 is a multipole[17]). The magnetic field in the median plane of this device can be expressed as

$$B = c_0 + c_1 x + c_2 x^2 + c_3 x^3 + c_4 x^4, \qquad (12)$$

where x is the horizontal distance from the center of the device. The various components are individually adjustable and this provides dynamic variables that affect mostly median-plane coefficients (x/θ, x/θ^2, $x/\theta\delta$, etc.) up to fourth order. The most important function of the multipole is to provide correction for the kinematic broadening discussed in section 6 below.

Another version of the Q3D spectrograph, the Q3DII[18]) (Brookhaven, Chalk River, Los Alamos, Saclay) has somewhat lower dispersion and a larger range: $p_{max}/p_{min} = 1.22$ versus 1.10 for Q3DI. Fig. 8 is a photograph of the Chalk River Q3DII.

The third dipole (D3) of Q3DI and Q3DII pro-

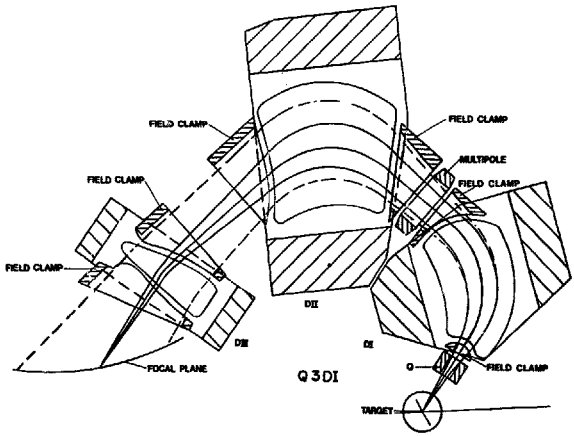

Fig. 7. Q3DI. The first of a series of "intermediate-image" spectrographs ($y/\phi=0$ in the multipole).

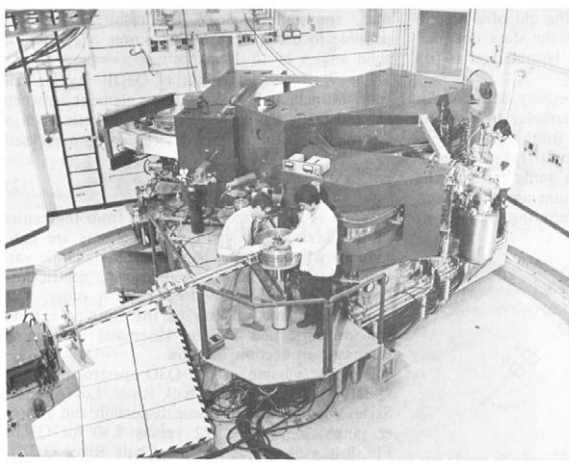

Fig. 8. Photograph of the Q3DII at Chalk River Laboratories, Canada.

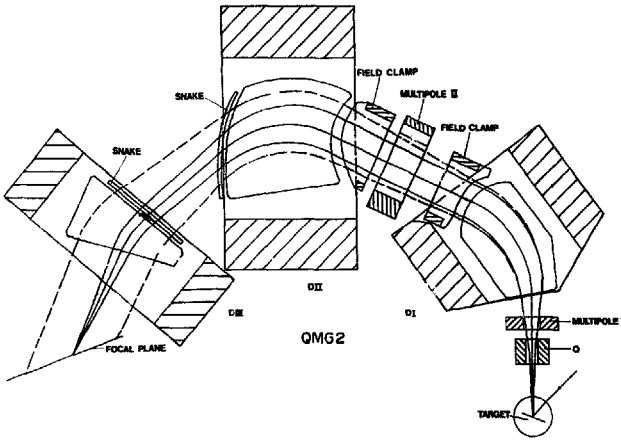

Fig. 9. The QMG2 (abbreviation for QMDMDD-Groningen 2). The curvatures of two of the boundaries can be adjusted with two sets of flexible equipotential bars, called snakes[21]).

vides most of the y-focusing between the intermediate and final images. In two other spectrographs of the Q3D series, the QWTH [19]) (Strasbourg) and the QMG2 [20,21]) (fig. 9 – Groningen, Berlin) the exit face of D2 does this job and D3 is used to make the term $(\theta/\delta)=0$ at the exit. This reduces the dispersion (and also D/M_x somewhat) and makes it possible to extend the range (QWTH). These two instruments also feature straight focal planes, and in the case of QMG2, practically linear calibration over the full range. Both instruments have been designed for operating with zero field in the central multipole for a kinematic factor $K=0.1$ (see section 6). For $K=0$ the multipole is "reversed". Finally, both have a first multipole, which is basically a sextupole with higher order corrections between the quadrupole and D1. The element provides dynamical adjustment of (x/θ^2), needed for optimum resolution when the kinematic factor K (section 6) is large. The central multipole is then used to recorrect terms such as $(x/\theta\delta)$ in addition to (x/θ). Figs. 10 and 11 show dispersion along the focal surface and D/M_x, respectively, for the various Q3D spectrographs.

All Q3D spectrographs mentioned above except the Brookhaven Q3DII were built by AB Scanditronix, Uppsala, Sweden. The Brookhaven instrument was built by Spectromagnetic Industries, Hayward, California.

In all Q3D spectrographs most of the corrections of the aberration coefficients are made on the di-

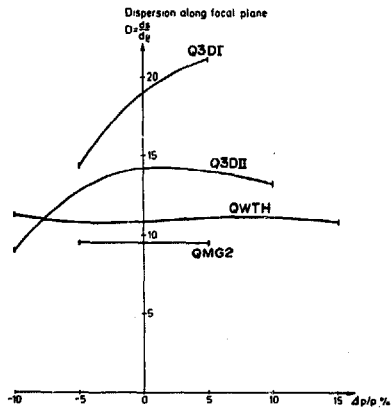

Fig. 10. Dispersion as measured along the focal surface for the Q3D spectrographs.

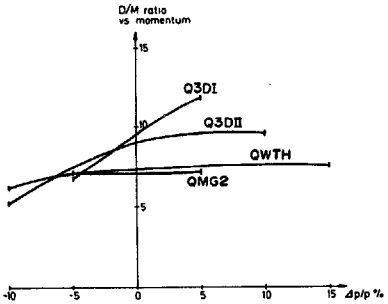

Fig. 11. D/M_x for the Q3D spectrographs.

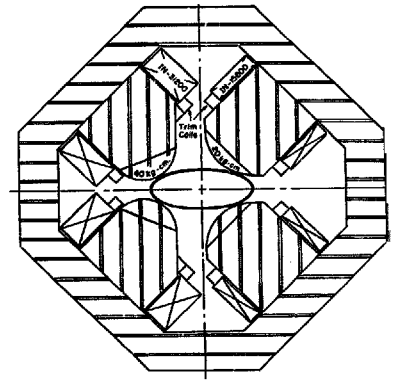

Fig. 12. The last quadrupole in the Indiana QDQ – with higher order corrections. Note the difference in ampere turns between the two sides: At nominal aperture radius $r=10$ cm the multipole field components are: $B_4=8.40$ kG, $B_6=-3.40$ kG, $B_8=1.56$ kG, and $B_{10}=0.60$ kG.

pole boundaries. The shapes of these boundaries are described as polonomials with the second-order term basically providing second-order corrections, etc. At least in one instance, terms up to eight order are used, not to correct (x/θ^8), which is not normally calculated, but terms such as $(x/\theta^5\delta^3)$. It is also feasible to make such corrections by distorting the field in quadrupoles. This is done in the QDQ (also called QDDM) spectrograph now in operation at the Cyclotron Facility of Indiana University[22]). The instrument was designed around an existing dipole. The pole pieces were replaced, and correction for (x/θ^2), (x/θ^3) and (x/θ^4) were produced partly by a small split cut as a groove across the pole pieces in the middle of the magnet, partly by pole-face windings. The latter also provide the quadrupole-type field needed for kinematic correction. The rest of the corrections needed are provided by the two quadrupoles both of which have quite strong higher order multipole fields superimposed upon the quadrupole fields. Fig. 12 is a cross sectional drawing of the last element of the Indiana QDQ.

Ikegami and coworkers[23]) at the Research Center for Nuclear Physics in Osaka, Japan, have designed a QDDQ which was built for them by Sumitomo Heavy Industries, Ltd. The central multipole has a strong enough quadrupole component so that it, together with the final quadrupole

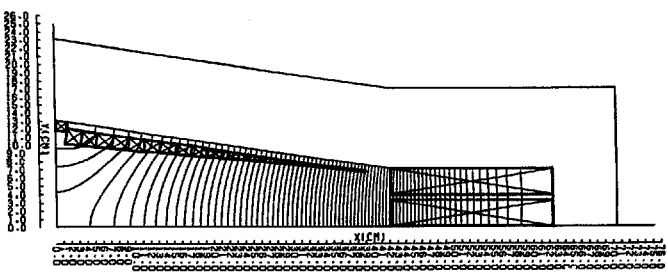

Fig. 13. The multipole in the Osaka QDDQ with quadrupole windings outlined. The field lines shown are for quadrupole excitation.

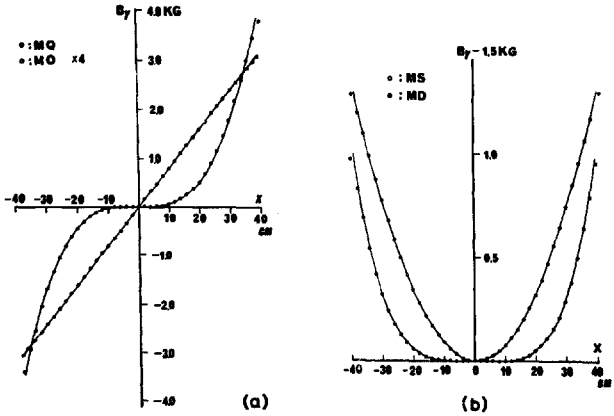

Fig. 14. Measured multipole fields vs x in the Osaka multipole [cf. eq. (12)].

forms a "zoom" lens which can be used to vary the dispersion by as much as 30%. Fig. 13 is a drawing of the central multipole with the distribution of the quadrupole conductors outlined. Fig. 14 shows the variation of B_y versus x as measured on the median plane ($y = 0$) for the various multipole components.

The spectrograph designer is always faced with a trade-off problem: dispersion versus range. There is a practical limit to the length of the focal surface (detector) of one to two times the length of the maximum orbit radius. So, clearly, large dispersion means small range and vice versa. Walcher[24]) accepted the challenge of designing a heavy-ion spectrograph with a dispersion that can be changed continuously by as much as a factor four. It can also correct for extreme cases of kinematic broadening (sec. 6). The instrument is a SQQDSQ where the S symbolizes a sextupole introduced for second-order corrections. It is being constructed for Gesellschaft für Schwerionenforschung (GSI), Darmstadt, West Germany.

A different challenge was met by the designers of a magnetic spectrograph for the cyclotron facility of the Kernforschungsanlage Jülich[25]). In order to match the energy capability of the cyclotron, the instrument needed to have dipole radii of 192 cm and dipole fields of $B = 18$ kG. To keep costs down, the designers had to keep the airgap and widths of pole faces to minima. They did it basically by vertical phase-space matching with a QQDDQ spectrograph (fig. 15). The quadrupole pair produces a horizontal image before the first dipole. A vertical image $(y/\phi) = 0$ is produced be-

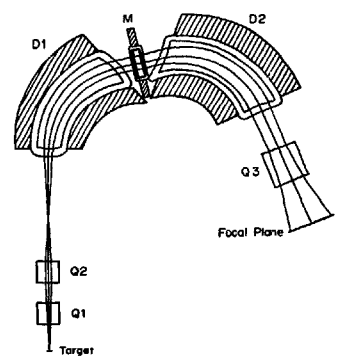

Fig. 15. The QQDDQ at the Kernforschungsanlage, Jülich, West Germany. Notice the horizontal cross-over $(x/\theta = 0)$ after Q1. A vertical image $(y/\phi) = 0$ occurs in the multipole M.

tween the two dipoles, as in the Q3D's. However, vertical *waists*, i.e. minimum beam envelopes, are formed inside both dipoles. The final quadrupole produces a y image on the detector. Since the (y/y) term is quite large inside the dipoles (maximum $|y/y| \approx 20$) careful attention has to be paid to the vertical position and spot size of the primary beam on the target. Aside from this the design parameters are excellent.

The split-pole spectrograph described above has a quite acceptable solid angle if only it could be fully utilized. The trouble is that the aberration term (x/θ^3) and also (x/θ^5), which was not calculated in the original design, are too large. An optical design has been made[26]) of a QSP* (SP for split-pole) with third- and higher-order corrections on the dipole boundaries as well as higher-order multipole terms in the quadrupole. The result is an instrument with quite acceptable characteristics (table 1). The focal plane is straight and the dispersion is constant. The QSP has not yet been built.

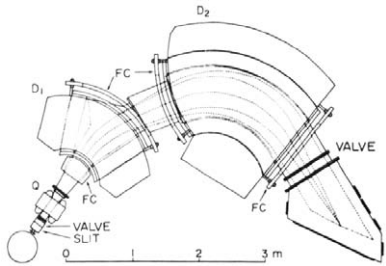

Fig. 16. The QDD at the Institute for Nuclear Study, University of Tokyo.

Kato and coworkers[27]) have designed a QDD for the Research Center for Nuclear Physics at the University of Tokyo. Fig. 16 shows the layout of the QDD and fig. 17 is a photograph of the same. The first-order optical parameters are listed in

* A QSP is not the same as a QDD because it has a field of, typically, one-seventh of the main field in the split, due to the common coil (fig. 5).

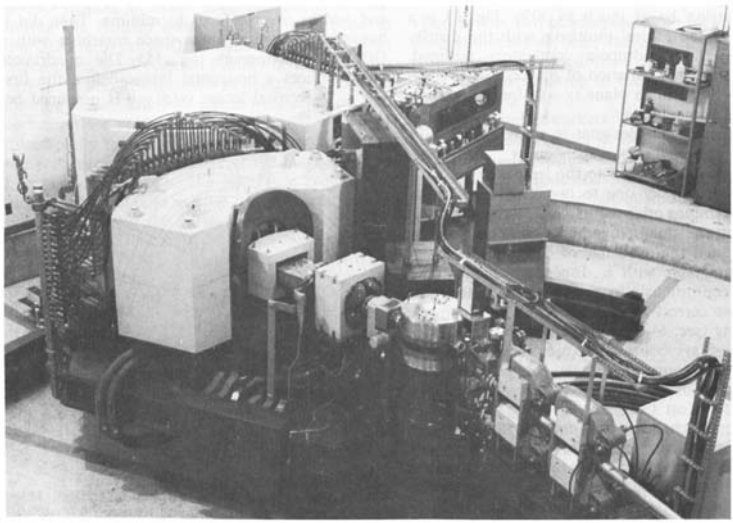

Fig. 17. Photograph of the Tokyo QDD.

table 1. Data on the aberrations were unavailable to this author at the time of writing.

As final entries in the list of single-gap spectrographs we mention four new designs, two of which are in the construction stage. All four designs were directed towards attainment of large acceptance solid angle.

A QDQ with no intermediate y-image is being built for the Instituut voor Kernphysisch Onderzoek (IKO) in Amsterdam[28]). It is to be used to detect hadrons in coincidence with electrons, analyzed by a different spectrometer. The dispersion D and D/M in this QDQ are smaller than for the intermediate-image instruments, but the parameters are otherwise quite good (table 1).

A pi-meson spectrograph with a 35 msr solid angle is presently being built for the University of Indiana. It is a QQSP[29]), with a relatively large dipole gap. The range is $p_{max}/p_{min} = 1.67$, and the focal plane is straight. All aberration terms are small except (x/θ^3) which has to be corrected in the data handling. This necessitates two detector planes.

Blomqvist[30]) has made optical studes of a QQSP with $(y/\phi) = 0$ in the split and $(y/y) \approx 0$ on the detector. The instrument is intended for vertical mounting such that the y position on the detector can be used as a measure of the reaction angle $(y/\phi \approx 0.6)$. The acceptance solid angle is 35 msr, and (x/ϕ^3) is small over most of the full range $p_{max}/p_{min} = 1.5$.

DeVries and Elmore[31]) have proposed a radically new type of instrument, intended for use in studies of heavy-ion reactions. It is a QD spectrograph with very large airgaps in both elements (superconducting coils). It would be mounted permanently at zero-degree relative to the beam. A forward cone of acceptance with reaction angles up to 40° can be handled. The beam would normally be stopped in a Faraday cup which removes a small central core of the acceptance cone. One large detector plane between the two elements and two beyond the dipole are to be used to "trace" the rays and determine their momenta and production angle.

6. Kinematic broadening

A magnetic spectrograph used to study nuclear reactions normally is required to focus particles leaving the residual nucleus in the *same state* to the same spot on the detector, independent of direction of emission. Therefore, a correction has to be made for the fact that the energy of these particles varies with angle. Otherwise, the result is *kinematic broadening* of the peaks in the energy spectrum and therefore loss of resolution. We define the kinematic factor K as:

$$K = -\frac{1}{p}\frac{dp}{d\theta_R}, \tag{13}$$

where θ_R is the reaction angle. The K-factor can be determined by differentiating the Q-value equation and the result is for the non-relativistic case

$$K = \frac{(M_i M_o E_i/E_o)^{\frac{1}{2}} \sin\theta_R}{M_o + M_R - (M_i M_o E_i/E_o)^{\frac{1}{2}} \cos\theta_R}. \tag{14}$$

Here, M_i, M_o, and M_R are the masses of the beam particle, the emitted particle, and the residual nucleus, respectively, and E_i and E_0 are the kinetic energies for beam and emitted particle.

Various methods can be used to correct for the kinematic broadening. In early experiments on the Kellogg spectrograph, which was mounted vertically, Mileikowsky[32]) showed that the kinematic broadening resulted in a slight slant of the lines formed on the nuclear track plate detectors. This occurred because the instrument was not exactly stigmatically focusing and, therefore, there was a correlation between the position on the nuclear track plate and the angle of emission from the target. In a later experiment, Smith and Enge[10]) showed that kinematic correction could be accomplished in a vertical QD spectrometer – the modified original Browne–Buechner instrument. A slight twist of the quadrupole about its axis produced the forces needed to accomplish the correction.

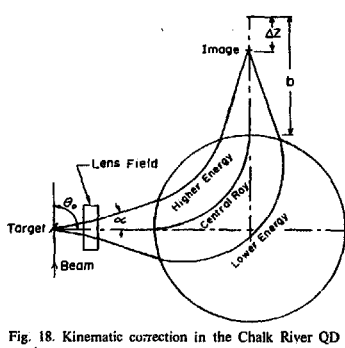

Fig. 18. Kinematic correction in the Chalk River QD Spectrograph.

In a horizontal QD spectrometer designed for Chalk River Laboratories in Canada[9]), the correction was accomplished by moving the detector closer to the magnet. How this produces the desired correction is shown schematically in fig. 18. A similar technique was used in the split-pole spectrograph[12]). It can easily be shown that the amount of detector displacement necessary for the correction is

$$\Delta z = -DM\rho K. \tag{15}$$

The minus sign implies scattering to the right and deflection to the left (as in fig. 18) or vice versa. For the split-pole $D \approx 2$ and $M_x \approx 1/3$ so for $K = 0.3$, for instance, we get $\Delta z \approx -0.2\rho$.

In the Q3D series of spectrographs, the dispersion is large and the magnification M_x is unity or larger. Therefore, the displacement as given by eq. (15) is very large even for moderate values of K. For these instruments a much more satisfactory method of correction is then to use a defocusing quadrupole element, preferably close to the middle of the spectrograph, to push the x-image back to the detector. As described above, this is one of the functions of the central multipole element. Not only is it used for producing a quadrupole field, but higher order multipole fields can also be introduced to correct for twisting and curving of the new focal surface, i.e. adjusting $(x/\theta\delta)$, $(x/\theta\delta^2)$, etc. in addition to (x/θ).

Fig. 19 shows two examples[33]) of kinematic correction obtained with a Q3DII spectrograph at full solid angle ($\Omega = 14.3$ msr). The residual peak widths are due mostly to target thickness effects.

In heavy-ion experiments the correction factor K can be quite large and it then becomes necessary to consider the effect of the angular spread of the beam and the resultant uncertainty in θ_R. This problem has been discussed in a report by Bohlen et al.[34]). The following analysis is essentially taken from their report.

The total angular spread of the beam $\Delta\theta_b$ can, of course, be varied by changing the ion-optical parameters of the beam-handling system. However, a reduction in the angular spread results in an increase in target spot size x_1, assuming a constant emittance $\varepsilon = x_1 \Delta\theta_b$ *. The contribution to the width of a peak in the energy spectrum from the angular spread is

$$\left(\frac{\Delta E}{E}\right)_{\theta_b} = 2\frac{\Delta p}{p} = 2K\Delta\theta_b = \frac{2K\varepsilon}{x_1}. \tag{16}$$

We combine this width quadratically with the width resulting from the imaging of the target spot size, x_1:

$$\left(\frac{\Delta E}{E}\right)_{x_1} = \frac{2M_x x_1}{DR}. \tag{17}$$

The result is

$$\frac{\Delta E}{E} = 2\sqrt{\left[\left(\frac{M_x x_1}{D\rho}\right)^2 + \left(\frac{K\varepsilon}{x_1}\right)^2\right]}. \tag{18}$$

In fig. 20 the energy resolution is plotted as a function of target spot size for an assumed emittance of $\varepsilon = 2\times10^{-6}$ rad·m and for $D\rho/M_x = 6.18$ m. Under these conditions the optimum target spot size for $K = 0.3$, for instance, is 2.1 mm and the maximum obtainable energy resolution is $E/\Delta E \approx 1100$ ($\mathcal{R} \equiv p/\Delta p \approx 2200$).

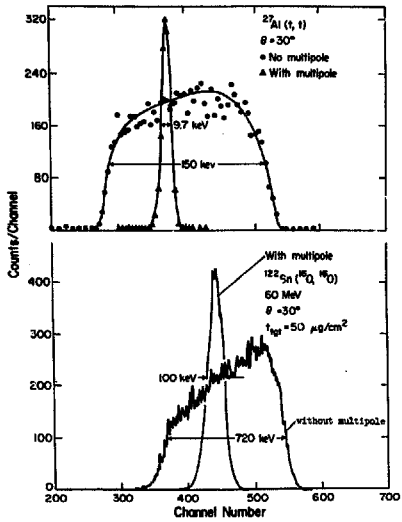

Fig. 19. The effect of kinematic correction by multipole in the Los Alamos Q3DII [33]).

* Emittance is usually defined as $\varepsilon = \frac{1}{2}\pi x_1 \frac{1}{2}\Delta\theta_b$. We have here absorbed the factor $\frac{1}{4}\pi$ into ε.

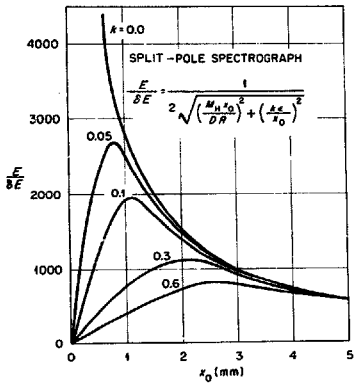

Fig. 20. The effect of beam emittance on the resolution. For large K-values, the best resolution is obtained with a relatively large target spot x_1 and therefore smaller beam divergence.

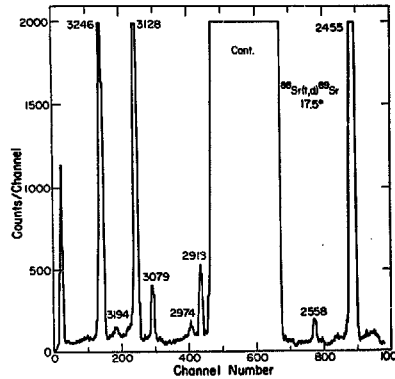

Fig. 21. Deuteron spectrum obtained with the Los Alamos Q3DII. Note the absence of "tails" on the intense peaks.

7. System resolution

The final energy resolution obtained with a magnetic spectrograph depends upon a number of other factors besides the aberration resolution [eq. (10)] and first-order resolution [eq. (8)]. Energy spread of the beam is one important contribution. Some beam handling systems have been designed such that they are "dispersion matched" with the spectrograph. Thereby, the contribution from beam energy spread can be largely eliminated. Since this technique is discussed in detail in the following paper by Bertozzi et al.[35]), we will not treat if further here. Other important contributions to the fwhm of the peaks in the energy spectrum are various factors attributable to the target and backing and to the angular spread of the beam (cf. section 6).

In many instances it is not enough to require that the fwhm of a peak in the energy spectrum is small but also that the *base* of the peak is well defined. This requires a low-aberration spectrograph, a well defined target spot, a clean and uniform target, and a beam without a low-energy "tail". Fig. 21 is a beautiful example of a spectrum with good base resolving power obtained with the Los Alamos Q3DII[35]). The peak at excitation energy $E_x = 2455$ keV is truncated and actually contains 2×10^5 total counts. Yet, the base is rather well defined. The broad truncated peak arises from carbon contamination and the large width is due to the fact that kinematic correction is made for the ^{88}Sr(t, d) reaction and not for the ^{12}C(t, d) reaction. Yet the base is well enough defined so that the small peaks to the left are discernable.

Target thickness effects are particularly important for heavy-ion reactions. The energy loss in even very thin targets is severe, straggling and multiple scattering bothersome. Ford[36]) has made a careful analysis of system resolving powers obtainable in practice for a number of heavy-ion reactions. The results are presented in table 2. Energy spread of the beam is not included.

The reactions are listed in column 1 and the beam energy in column 2. The target thickness and backing (if any) are given in column 3. Columns 4 and 5 give the results of energy and charge straggling in the target and the backing, and columns 6 and 7 are the results of presumed non-uniformities of the target and the backing. The total energy loss in the target does not enter directly but rather the difference in energy loss between the incident particle and the scattered particle. At 20° scattering angle and with the target set at 10°, this contribution is generally not dominant (column 8). Listed next, in columns 9 and 10, are the effects of multiple scattering of the incident and emitted particles in the target and

TABLE 2

Obtainable resolving powers for various heavy-ion reactions.

1 Reaction	2 Energy (MeV)	3 Target thickness ($\mu g/cm^2$)	4 Energy and charge straggling Target (keV)	5 Backing (keV)	6 Target nonuniformities Target (keV)	7 Backing (keV)	8 Target ΔE difference (keV)	9 Multiple scattering Target (keV)	10 Backing (keV)	11 Total energy spread due to target (keV)	12 Effect of beam emittance (keV)	13 Total energy spread (keV)	14 Energy resolution $E/\Delta E$
$^{12}C(^{12}C, ^{12}C)$	100	10	20		4		2	16		26	99	102	1000
	175	10	20		2		1	16		26	174	176	1000
$^{12}C(^{12}C, \alpha)$	100	10	20		4		15	6		26	61	66	1500
	175	10	20		2		10	7		23	108	110	1600
$^{24}Mg(^{12}C, ^{12}C)$	100	10 on 10C	20	20	3	4	1	9	16	34	69	77	1300
	175	10 on 10C	20	20	2	2		16	16	36	120	125	1400
$^{24}Mg(^{12}C, \alpha)$	100	10 on 10C	20	20	3	4	13	4	16	46	47	59	1700
	175	10 on 10C	20	20	2	2	8	4	16	34	83	89	2000
$^{58}Ni(^{12}C, ^{12}C)$	100	10 on 10C	20	20	3	4		5	16	33	47	57	1800
	175	10 on 10C	20	20	2	2		5	16	33	82	88	2000
	175	50	45		8			15		48	82	95	1800
$^{58}Ni(^{12}C, \alpha)$	175	10 on 10C	20	20	2	2	8	3	16	34	57	66	1500
	175	50	45		8		39	4		60	57	83	2100
$^{120}Sn(^{12}C, ^{12}C)$	100	10 on 10C	19	20	2	4		2	16	32	31	45	2200
	175	10 on 10C	19	20	2	2		2	16	32	54	63	2800
	175	50	42		8			6		43	54	69	2500
$^{120}Sn(^{12}C, \alpha)$	175	10 on 10C	19	20	2	2	8	1	16	33	40	52	3400
	175	50	42		8		40	4		58	40	70	2500
$^{58}Ni(^{28}Si, ^{28}Si)$	225	50	104		27			73		130	155	202	1100
$^{107}Ag(^{40}Ca, ^{40}Ca)$	375	10 on 10C	64	68	14	25		24	100	143	233	273	1400
	375	50	142		35			86		169	233	288	1300
$^{153}Eu(^{40}Ca, ^{40}Ca)$	180	50	138		32			27		145	89	170	1100
	360	50	138		35			55		152	179	235	1500
$^{197}Au(^{58}Ni, ^{58}Ni)$	200	50	190		50			42		203	105	229	900
	400	50	190		60			84		214	211	301	1300
$^{197}Au(^{90}Zr, ^{90}Zr)$	225	50	271		87			92		300	148	335	700
	450	50	271		90			184		340	296	451	1000

backing. The mechanism is that a change in the direction gives a non-correctible contribution to the kinematic broadening. The total energy spread from all target effects added quadratically is given in column 11. Column 12 shows the effect of beam emittance calculated with the aid of the analysis in section 6 with $\varepsilon = 2 \times 10^{-6}$ rad·m and $Dp/M_x = 6.18$ m. In each case it has been assumed that the target spot size x_1 is optimum.

The entries in columns 11 and 12 have been added quadratically. The results are given in column 13 with the corresponding energy resolution in column 14. As outlined above, the first-order contribution of the spectrograph (with $Dp/M_x = 6.18$ m) has been built into the analysis giving the numbers in column 12. Assuming that a spectrograph with perfect kinematic correction and very low aberration is employed, the numbers in column 14 represent the final resolution (for the listed target thicknesses). With a less-than-perfect

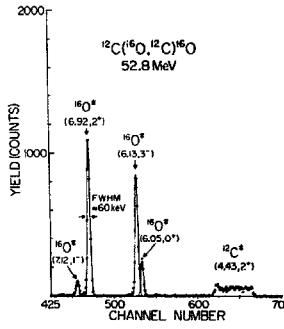

Fig. 22. Spectrum of ^{12}C ions observed by bombarding a carbon target with an oxygen beam. Instrumentation: split-pole spectrograph and Rochester heavy-ion detector.

spectrograph these resolution values can always be reached by reducing the solid angle.

Fig. 22 shows as an example a ^{12}C spectrum obtained with the Rochester MP Tandem and split-pole spectrograph[37]). The broad peak arises from a collision leaving ^{16}O in its ground state and ^{12}C in its first excited state, decaying in flight with resulting Doppler broadening.

8. Multigap spectrographs

The original MIT Browne–Buechner spectrograph was employed in a large number of stripping reactions and other charged-particle reaction studies in which it was desirable to get detailed angular-distribution data. Target breakage was always a problem, and hardly any angular distribution was completed with the same target. Overlapping runs had to be made for normalization purposes. Targets also collect surface contamination gradually and some deteriorate gradually. W. W. Buechner and the present author carried on a continued discussion about this problem in 1955/56. The solution found eventually was the multigap spectrograph announced first in a 1956 MIT Progress Report[38]). Credit must be given to R. Middleton[39]) who adopted the idea a year later and had a working Multigap at Aldermaston, England long before the MIT instrument was completed.

The MIT Multigap has been described in detail in a paper by Enge and Buechner[40]). Since some of the later instruments have additional features, we select one of them, the Yale instrument[41]), for a closer look.

Fig. 23 is a simplified drawing showing two views of the Yale Multigap. The toroidal magnetic circuit is made of forty-eight 7.5° cast-iron wedges some of which are thinner than others so as to leave gaps between them. The segments are clamped together to form a toroid with stainless steel spacers defining the gaps. Each gap is $\frac{1}{4}$" wide and magnetized by the coils on the two adjacent poles. Each segment adjacent to a gap has two coils of five turns each with the exception of the outside segment of the "end" gaps which has only one coil of five turns and a "magnetic mirror" to terminate the fringing field flowing through the coils, but outside the iron.

The target is in the center of the torus and the beam enters through one of the three "field free" holes through the iron. The torus can be rotated to any of three orientations which place gap 1 at

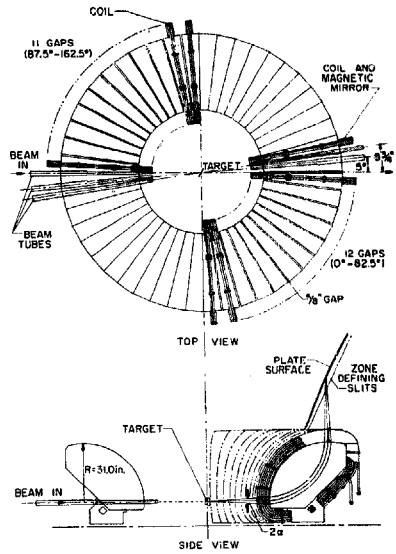

Fig. 23. Schematic drawings of the Yale Multigap. The magnet is basically a torus with airgaps and coils in two of the quadrants. The beam enters through one of three practically field free holes in the iron.

0°, 5°, or $8\frac{3}{4}$° to the beam. This, in practice, gives the experimenter a choice between a set of angles spaced 7.5° apart and starting at 7.5°, and another set spaced 3.75° apart and starting at 5°. For the second choice, two exposures are required.

From fig. 23 one can also see the characteristic Browne–Buechner geometry which is identical for all gaps. The pole face radius is 31" and the spectrograph was designed with an effective pole face radius of 31.625" ($R = R_0 + \varepsilon d$; where $\varepsilon = 1.0$ and $d = \frac{5}{8}$"). The range of energy covered in one exposure is approximately 2.5:1 corresponding to 85 MeV protons at the top and 34 MeV protons at the bottom for a maximum field of 15 kG. The design calls for one inch wide nuclear track plates of 48" total length. In one gap (#15, at approximately 110°) there is an NMR probe used to determine and control the field.

Fig. 24 gives a more detailed view of the spec-

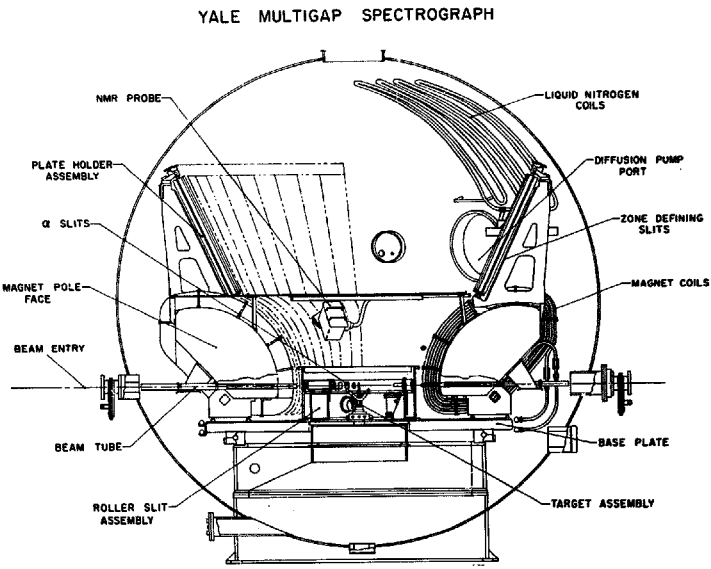

Fig. 24. More detailed side view of the Yale Multigap. The complete assembly can rotate through 8½° about its vertical axis so that any of the three beam ports shown in fig. 23 can be selected.

trograph showing the vacuum sphere as well as some other mechanical details. The nuclear track plate detectors are supported by individual plate holders and conform to the hyperbolic surface of the holders by spring mechanisms. Each gap has a rotating spine with provisions for three plate loads. The spines can be remotely rotated into position for exposure.

The target assembly allows for three targets, although in practice one location is used for the purpose of focusing the beam at the multigap center. The target assembly can be rotated about the center for various orientations to the beam. The reaction products leave the scattering chamber through the slits mounted on the scattering chamber wall. A shutter ring which can rotate to three orientations allows one to close the slits, or choose either normal slits ($\alpha = 2.6°$) or Rutherford slits (α modified by the $\sin^{-4}\frac{1}{2}\theta$ factor). The Rutherford slits are used only in the forward quadrant. Mounted in front of each nuclear track plate holder are slits defining an exposure zone of constant width. The solid angle at 90° deflection using normal slits ($\alpha = 2.6°$) is approximately 3.6×10^{-4} sr.

The multigap spectrographs have three major advantages over single-gap spectrographs for work in which accurate angular distributions are important:

1) Increased data-taking power. Not only is the exposure time cut down drastically, but there is no wasted beam time for changing angle and, in the case that nuclear emulsions are used, for re-loading.

2) Increased accuracy of relative cross-section measurements (angular distributions). Target deterioration and collection of surface contamination affect all angles in identical fashion.

3) Angles much closer to 180° can be covered – typically 172.5° for the Multigap versus 135° for a vertical single-gap spectrograph and 160°

TABLE 3
Multigap spectrographs.

Location	Type	Pole piece radius (cm)	Maximum orbit radius (cm)	Airgap (cm)	No. of active gaps	Angular separation (degrees)	No. of beam ports	Smallest angular interval (degrees)	Exposures per load
MIT	B-B	50	57	1.0	24	7.5	1	7.5	3
Aldermaston	B-B	50.8	58	1.3	24	7.5	1	7.5	1
Mexico	B-B	60	68	1.0	18	10	1	10	3
Oxford	B-B	61.0	69	1.3	24	7.5	2	3.75	2
U. of Penn.	B-B	61.0	69	1.3	24	7.5	2	3.75	2
Yale	B-B	78.7	90	1.6	23	7.5	3	3.75	3
Heidelberg	B-B	78.7	90	1.6	29	7.5	3	3.75	3
Niels Bohr Inst.	Elbek	–	100	2.0	26	10	1	5	2

for a horizontal instrument, such as the split-pole.

Seven multigap spectrographs have been built of the Browne–Buechner type and one of the Elbek type. The most important features of these seven instruments are given in table 3.

References

1) J. D. Cockroft, J. Sci. Instr. 10 (1933) 71.
2) K. L. Brown and S. K. Howry, Stanford Linear Accelerator Report SLAC 91.
3) S. B. Kowalski and H. A. Enge, unpublished. Short descriptions given in refs. 12, 15 and 20.
4) W. W. Buechner, E. N. Strait, C. G. Stergiopoulos and A. Sperduto, Phys. Rev. 74 (1948) 1569. Also: W. W. Buechner, R. J. Van de Graaff, E. N. Strait, C. G. Stergiopoulos and A. Sperduto, Phys. Rev. 74 (1948) 1226.
5) H. A. Enge, W. W. Buechner, A. Sperduto and D. M. Van Patter, Phys. Rev. 83 (1951) 31.
6) C. W. Snyder, C. C. Lauritsen, W. A. Fowler and S. Rubin, Phys. Rev. 74 (1948) 1564.
7) J. Bardwick, J. M. Lambert and W. C. Parkinson, Nucl. Instr. and Meth. 18-19 (1962) 105.
8) C. P. Browne and W. W. Buechner, Rev. Sci. Instr. 27 (1956) 899. Also: W. W. Buechner, C. P. Browne, H. A. Enge, A. Sperduto, M. Mazari and C. D. Buntschuh, Phys. Rev. 95 (1954) 609.
9) H. A. Enge, Rev. Sci. Instr. 29 (1958) 885.
10) D. L. Smith and H. A. Enge, Nucl. Instr. and Meth. 79 (1970) 144.
11) J. Borggren, B. Elbek and L. P. Nielsen, Nucl. Instr. and Meth. 24 (1963) 1.
12) J. E. Spencer and H. A. Enge, Nucl. Instr. and Meth. 49 (1967) 181. Also: H. A. Enge, Nucl. Instr. and Meth. 28 (1964) 19.
13) R. M. DeVries, D. Shapira and M. R. Clover, Nucl. Instr. and Meth. 140 (1977) 479.
14) D. L. Hendrie, J. R. Meriwether, F. Selph, D. Morris and C. Glasshausser, Bull. Am. Phys. Soc. 15 (1970) 650. More details in F. Selph, Engineering Note UCID-3388, Lawrence Radiation Laboratory, Univ. of Cal. (Sept. 22, 1969).
15) H. A. Enge and S. B. Kowalski, Proc. Int. Conf. on *Magnet technology*, Hamburg (1970) p. 366. Also: H. A. Enge, U.S. Patent 3 541 328.
16) C. A. Wiedner, M. Goldschmit, D. Rieck, H. A. Enge and S. B. Kowalski, Nucl. Instr. and Meth. 105 (1972) 205. Also: M. Löffler, H. J. Scherrer and H. Vonach, Nucl. Instr. and Meth. 111 (1973) 1.
17) H. J. Scherrer, H. Vonach, M. Löffler, A.v.d. Decken, M. Goldschmidt, C. A. Wiedner and H. A. Enge, Nucl. Instr. and Meth. 136 (1976) 213. See also ref. 15.
18) M. J. LeVine and H. A. Enge, Bull. Am. Phys. Soc. 15 (1970) 1688.
19) H. A. Enge and R. Rebmeister, unpublished.
20) A. G. Drentje, H. A. Enge and S. B. Kowalski, Nucl. Instr. and Meth. 122 (1974) 485.
21) A. G. Drentje, R. J. deMeijer, H. A. Enge and S. K. Kowalski, Nucl. Instr. and Meth. 133 (1976) 209.
22) R. D. Bent, D. G. Madland, J. D. Cossairt, A. D. Bacher, W. P. Jones, D. W. Miller, R. E. Pollock and P. Schwandt, Indiana University Cyclotron Facility Report No. 1-73. Also: H. A. Enge and S. B. Kowalski, unpublished report.
23) H. Ikegami, S. Morinobu, I. Katayama, M. Fujiwara, Y. Fujita and H. Ogata, Annual Report 1976, Research Center for Nuclear Physics, Osaka University, p. 113.
24) T. Walcher, MPI-Sonderdruck MPI H-1974-V25, Heidelberg (1974).
25) A. Abdel-Gawad, A. Hardt, S. Martin, J. Reich, K. L. Brown and K. Halbach, Proc. Int. Conf. on *Magnet technology*, Rome (1975) p. 45.
26) H. A. Enge, unpublished report.
27) S. Kato, T. Hasegawa and M. Tanaka, to be published.
28) J. C. Bergstrom, P. J. T. Bruinsma, R. C. Hicks, C. W. de Jager, H. de Vries, H. van de Watering-Obluska, Annual Report 1975, IKO, Amsterdam, p. 17. Also: H. A. Enge and S. B. Kowalski, unpublished report.
29) H. A. Enge, S. B. Kowalski and W. Jones, unpublished report.
30) I. Blomqvist, work in progress.
31) R. M. DeVries and D. Elmore, University of Rochester Report UR-NSRL-142.
32) C. Mileikowski, private communication.
33) E. R. Flynn, S. Orbesen, J. D. Sherman, J. W. Sunier and R. Woods, Nucl. Instr. and Meth. 128 (1975) 35.
34) D. H. Bohlen, G. Gebauer and W. von Oertzen, Vorschlag

für ein Magnetspectrometer für VICKSI, Hahn Meitner Institut, Berlin, HMI-B 171.
[35]) W. Bertozzi, M. W. Hynes, C. P. Sargent, W. Turchinetz and C. F. Williamson, following paper.
[36]) J. L. C. Ford, Jr., H. A. Enge, J. R. Erskine, D. L. Hendrie and M. J. LeVine, ORNL/TM-5687.
[37]) D. Shapira, R. M. DeVries, M. R. Clover, R. N. Boyd and R. N. Sherry, Jr., Phys. Lett. 71B (1977) 293.
[38]) H. A. Enge, C. H. Paris, M. Mazari and W. W. Buechner, Progress Reports, Lab. for Nucl. Sci., MIT (Feb. 1957 and May 1957).
[39]) R. Middleton and S. Hinds, Nucl. Phys. 34 (1962) 404.
[40]) H. A. Enge and W. W. Buechner, Rev. Sci. Instr. 34 (1963) 155.
[41]) D. G. Kovar, C. K. Bockelman, W. D. Callander, L. J. McVay, C. F. Maguire and W. D. Metz, Wright Nuclear Structure Laboratory, Yale University, Internal Report no. 49.